

# Remotely Triggered Seismicity in the Yellowstone National Park Region by the 2002 $M_w$ 7.9 Denali Fault Earthquake, Alaska

by Stephan Husen, Stefan Wiemer, and Robert B. Smith

**Abstract** Coincident with the arrival of low-frequency, large-amplitude surface waves of the  $M_w$  7.9 Denali fault earthquake (DFE), an abrupt increase in seismicity was observed in the Yellowstone National Park region, despite the large epicentral distance of 3100 km. Within the first 24 hr following the DFE mainshock, we located more than 250 earthquakes, which occurred throughout the entire Yellowstone National Park region. The elevated seismicity rate continued for about 30 days and followed a modified Omori law decay with a  $P$  value of  $1.02 \pm 0.07$ . For a declustered earthquake catalog, the seismicity following the 2002 DFE uniquely stands out with a significance of  $30\sigma$ . The increase in seismicity occurred over all magnitude bands. In general, we observed that seismicity following the DFE outlined the spatial pattern of past seismicity routinely observed in the Yellowstone National Park region. However, we found significant differences in triggered seismicity inside and outside the caldera. Earthquakes inside the Yellowstone caldera occurred preferentially as clusters close to major hydrothermal systems, were of larger magnitude, and seismicity decayed more rapidly. This suggests that either different trigger mechanisms were operating inside and outside the caldera or that the crust responded differently to the same trigger mechanism depending on its different mechanical state. Compared with other sites that experienced remote earthquake triggering following the 2002 DFE, Yellowstone showed the most vigorous earthquake activity. We attribute this to strong directivity effects of the DFE, which caused relatively large peak dynamic stresses (0.16–0.22 MPa) in Yellowstone, and to the volcanic nature of Yellowstone.

## Introduction

An abrupt increase in seismicity in many areas of the western United States following the  $M_w$  7.3 1992 Landers earthquake provided the first widely accepted evidence for the phenomenon of triggering of local earthquakes at distances of several fault lengths (Hill *et al.*, 1993; Anderson *et al.*, 1994; Bodin and Gomberg, 1994). Since the 1992 Landers earthquake, only a few more examples of remote earthquake triggering have been observed. For example, the 1999  $M_w$  7.1 Hector Mine earthquake triggered earthquakes at distances of several fault lengths, but triggering was more directed to the south compared with the 1992 Landers earthquake (Gomberg *et al.*, 2001). Other, less well documented, examples of remotely triggered seismicity after large earthquakes were detected at the Geysers geothermal field, California, including the 1988  $M_s$  7.6 Gulf of Alaska, the 1989  $M_s$  7.1 Loma Prieta, and the  $M_w$  7.3 1992 Landers earthquakes (Stark and Davis, 1996). Although there is a tendency for remote earthquake triggering to occur at sites of geothermal and recent volcanic activity, an example of remotely triggered earthquakes in a non volcanic area was reported from Greece following the 1999  $M_w$  7.4 Izmit, Tur-

key, earthquake, at distances from 400 km to nearly 1000 km (Brodsky *et al.*, 2000).

The cause of remotely triggered seismicity remains unclear. Because static stress changes fall below daily tidal stress changes at large distances ( $>300$  km), dynamic stress changes associated with large-amplitude surface waves are considered to be important for remote earthquake triggering (Hill *et al.*, 1993). A number of models have been proposed to transfer dynamic stress changes into sustained stress changes capable of triggering earthquakes (for an overview see Hill *et al.*, 2002), but owing to limited observations none of the models can be ruled out. The occurrence of the 1999  $M_w$  7.1 Hector Mine earthquake, close to the location of the 1992 Landers earthquake, provided a rare opportunity to compare remote earthquake triggering at locations that experienced earthquake triggering for both earthquakes. Peak dynamic velocities or stresses recorded at sites that experienced earthquake triggering for both large earthquakes suggested the existence of dynamic triggering thresholds (Gomberg *et al.*, 2001).

The 2002  $M_w$  7.9 Denali fault earthquake (DFE), Alaska,

was the largest strike-slip earthquake to occur in North America in almost 150 years (Eberhart-Phillips *et al.*, 2003). A total of 340 km of surface rupture occurred, and the maximum observed surface offset was 8.8 m (Eberhart-Phillips *et al.*, 2003). The long, unilateral slip resulted in strong rupture directivity in both the teleseismic *S* waves and the surface waves that propagated toward the southeast along the strike of the Denali and Totschunda faults (Eberhart-Phillips *et al.*, 2003; Velasco *et al.*, 2004). The DFE triggered swarms of earthquakes in locations throughout most of the western United States up to 3660 km from its epicenter. These were concentrated largely at volcanic sites, including (1) the Katmai volcanic field in Alaska (Moran *et al.*, 2004), (2) Mt. Rainier in central Washington (Prejean *et al.*, 2004), (3) the Geysers in northern California (Prejean *et al.*, 2004), (4) the Long Valley caldera in eastern California (Prejean *et al.*, 2004), (5), and the Coso geothermal field in southeastern California (Prejean *et al.*, 2004). However, earthquake triggering was also observed at nonvolcanic areas along the Wasatch fault zone in Utah (Pankow *et al.*, 2004) and in Montana and Idaho (Husker and Brodsky, 2004). Thus, the DFE provided the most thoroughly documented and most far-reaching case of remote earthquake triggering observed to date. In this article, we report on remote earthquake triggering in the Yellowstone National Park region (Yellowstone) following the 2002  $M_w$  7.9 DFE. We describe the temporal and spatial evolution of remotely triggered seismicity and provide estimates on the statistical significance and on the duration of this seismic sequence. Finally, we compare our results with remote earthquake triggering documented at other sites and discuss possible trigger mechanisms at Yellowstone.

### Tectonic Setting and Background Seismicity in Yellowstone

The Yellowstone volcanic field, centered within the Yellowstone National Park, is one of the largest silicic volcanic systems in the world (Smith and Siegel, 2000; Christiansen, 2001). The youthful volcanic history of Yellowstone was dominated by three cataclysmic caldera-forming eruptions in the past two million years (Christiansen, 2001). The most recent eruption, 0.64 million years ago, formed the present-day 40 × 60-km-long Yellowstone caldera (Fig. 1). Since the last cataclysmic eruption, at least 30 dominantly rhyolitic and basaltic flows as young as 70,000 years have been erupted, covering much of Yellowstone (Christiansen, 2001). Yellowstone is still considered volcanically active, as indicated by its large hydrothermal system, its high seismicity with over 20,000 earthquakes since 1973, and its episodes of caldera-wide deformation (Pelton and Smith, 1979; Dzurisin *et al.*, 1994; Wicks *et al.*, 1998). With over 10,000 geysers, hot springs, and fumaroles, Yellowstone has the world's highest concentration of hydrothermal features. Yellowstone's expansive hydrothermal system is considered to arise from hot water circulating along fracture systems in the

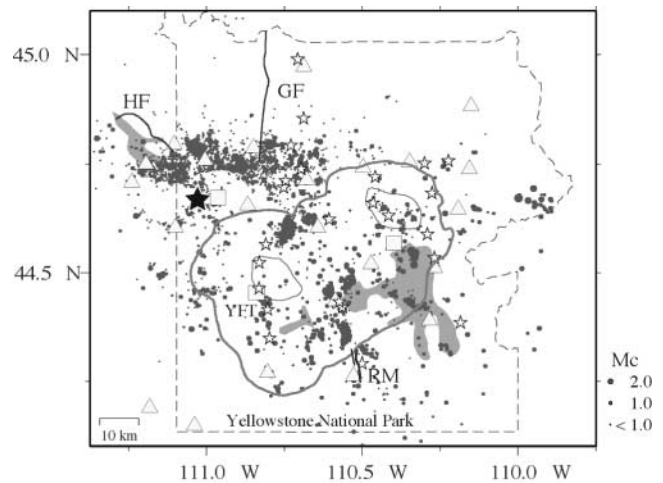


Figure 1. Background seismicity in Yellowstone (2000–2001). Epicenter locations are scaled by coda magnitude,  $M_c$ , as indicated. Stations of Yellowstone seismic network are shown as gray triangles (short-period, one-component) and gray squares (broadband, three-component). Gray stars mark mapped hydrothermal features. The thick gray line denotes 0.64  $M_a$  Yellowstone caldera; thin gray lines denote resurgent domes. Outline of Yellowstone National Park (dashed line) is shown for reference. Location of 1985 earthquake swarm is shown as black star. Major normal faults are shown by thick black lines: RM, Red Mountain fault zone; GF, Gallatin fault; HF, Hebgen and Red Canyon faults.

upper crust and heated by crystallizing magma, 10–15 km deep (Fournier, 1989). Most of the hydrothermal features are located inside the Yellowstone caldera close to two resurgent domes and along a fault zone extending northward from Norris geyser basin (Fig. 1).

Seismicity in Yellowstone has been routinely recorded at a permanently installed seismic network since 1973 (Pitt, 1987; Nava and Smith, 1996; Husen and Smith, 2004c). Since 1995 the network has consisted of six three-component seismometers and 19 one-component seismometers; three of the sites were equipped with broadband seismometers (Fig. 1). Earthquake data are transferred to the University of Utah Seismograph Stations (UUSS), Salt Lake City, Utah, via analog telemetry, except for data from the broadband seismometers, which are digitally telemetered. Travel-time picks are routinely determined by an analyst at the UUSS, and hypocenter locations are obtained through linearized earthquake location techniques using one-dimensional velocity models (Nava and Smith, 1996; Husen and Smith, 2004). Seismicity in Yellowstone is concentrated mostly in the northwestern region outside the Yellowstone caldera (Fig. 1). Within the Yellowstone caldera seismicity is more diffuse but individual clusters of earthquakes can be associated with major hydrothermal areas (Husen and Smith, 2004c) (Fig. 1). Focal depths show a notable shallowing within the Yellowstone caldera, possibly related to elevated temperatures beneath

the caldera due to the presence of crystallizing magma (Smith and Arabasz, 1991; Miller and Smith, 1999). Large earthquake swarms are common in Yellowstone, occurring primarily in the northwestern region outside the Yellowstone caldera. The largest recorded swarm in Yellowstone occurred in October 1985 with over 3000 earthquakes (Fig. 1). The occurrence of this earthquake sequence has been related to the migration of hydrothermal fluids radially outward from the Yellowstone caldera following the rupture of a sealed hydrothermal system within the caldera (Waite and Smith, 2002).

### Spatial and Temporal Evolution of Remotely Triggered Earthquakes in Yellowstone

To map and analyze remotely triggered seismicity following the DFE, we relocated the seismicity following the DFE using three-dimensional velocity models and the nonlinear earthquake location technique NonLinLoc. (Lomax *et al.*, 2000). The improved velocity models and nonlinear earthquake location resulted in better focal depth estimates and tighter clustering as compared to routinely obtained earthquake locations (Husen and Smith, 2004). Coda magnitudes ( $M_c$ ) were recomputed using the same improved coda magnitude equation for all earthquakes (Pechmann *et al.*, 2001). Calibrating  $M_c$  against Richter local magnitudes  $M_L$  yield average  $M_c - M_L$  differences of less than 0.1 magnitude units for  $M_L < 4.0$  earthquakes (Pechmann *et al.*, 2001). Consequently, our coda magnitudes are comparable to Richter local magnitudes.

Figure 2 displays relocated seismicity as observed within 30 days following the DFE. Within 24 hr after the DFE, earthquakes were triggered throughout most of Yellowstone. Triggered seismicity occurred primarily at sites that were previously seismically active, including hydrothermal areas within the Yellowstone caldera and the northwestern region outside the Yellowstone caldera. Focal depths of triggered earthquakes follow the same trend of the past seismicity, with shallower focal depths inside the Yellowstone caldera (Fig. 2b,c).

To determine the exact onset of triggered seismicity, we high-pass filtered broadband recordings of station YFT, located within the Yellowstone caldera close to Old Faithful geyser in Upper geyser basin (Fig. 1). Local earthquake activity began with the arrival of long-period, large-amplitude Love waves at 22:26 UTC on 3 November 2002, 14 min after the DFE mainshock (Fig. 3). Peak dynamic stresses at YFT associated with Love and Rayleigh waves were on the order of 0.22 MPa (Velasco *et al.*, 2004). The first 10 min following the arrival of the surface waves were characterized by bursts of small earthquakes including one larger event of  $M_c > 2.0$ , which occurred well after the passage of the Rayleigh waves. We were not able to locate or determine reliable magnitudes for these early triggered events, because all of the analog-telemetered seismic stations became saturated owing to the large amplitudes of the surface waves. The

magnitude of the largest event within the first 10 min was estimated by comparing amplitudes in the seismogram using the first located earthquake at 22:40 with  $M_c$  0.9 (Fig. 3b). Locating earthquakes within the first 6 hr following the DFE was complicated by the fact that many of the triggered earthquakes occurred simultaneously throughout Yellowstone (Fig. 2). As a result, we located only earthquakes with consistent arrival times that could be discriminated by the seismic analyst at more than six azimuthally well-distributed seismic stations. This principally affected smaller earthquakes that were recorded only at close stations.

Seismicity triggered by the DFE was sustained and continued well beyond the passage of the DFE surface waves. We were able to locate more than 250 earthquakes within the first 24 hr following the DFE. Seismicity gradually decayed over the subsequent weeks (Fig. 4). One exception is the occurrence of a small earthquake swarm of more than 20 events on 11 November 2002, 8 days after the DFE. This swarm sequence took place close to West Thumb geyser basin, one of the major geyser basins in Yellowstone (Fig. 2). Magnitudes of triggered earthquakes ranged from  $< 0.0$  to 3.2. The largest event, having  $M_c$  3.2, occurred beneath the northern end of the Yellowstone Lake (Fig. 2), 78 min after the DFE. Some of the initial events were felt by National Park Service employees, who were the only people in Yellowstone at that time. Within 24 hr following the DFE, 11 earthquakes with  $M_c > 2.5$  were recorded compared to nine earthquakes with  $M_c > 2.5$  in all of 2002 prior to the DFE.

Within the first 2 hr following the DFE, earthquakes clustered close to three major hydrothermal areas in Yellowstone (Fig. 5): (1) at Upper geyser basin, (2) at West Thumb geyser basin, (3) and at the north end of Yellowstone Lake. While Upper and West Thumb geyser basins are well known for their concentration of geysers and hot springs, active hydrothermal features beneath the northern end of Yellowstone Lake were recently detected from multibeam sonar mapping and seismic reflection surveys (Morgan *et al.*, 2003). The earthquake activity following the DFE at these hydrothermal areas was extremely vigorous compared to the low level of background seismicity in 2002 (Fig. 6). A relatively large number of triggered earthquakes had magnitudes  $> 2$  (Fig. 7). Shallow focal depths ( $< 5$  km) and epicenter locations that were offset from the actual surface locations of the hydrothermal areas (Fig. 6) suggest that these earthquakes were triggered close to hydrothermal reservoirs and not at individual geysers. Geochemical analysis proposed that these hydrothermal reservoirs might exist at an intermediate depth beneath individual geyser basins (Fournier, 1989). Seismicity triggered at Upper and West Thumb geyser basins and beneath the northern end of Yellowstone Lake decayed rapidly; 24 hr after the DFE only a few small earthquakes were observed at these sites (Fig. 7). The only exception is West Thumb geyser basin, where an earthquake swarm of similar intensity (magnitudes and number of earth-

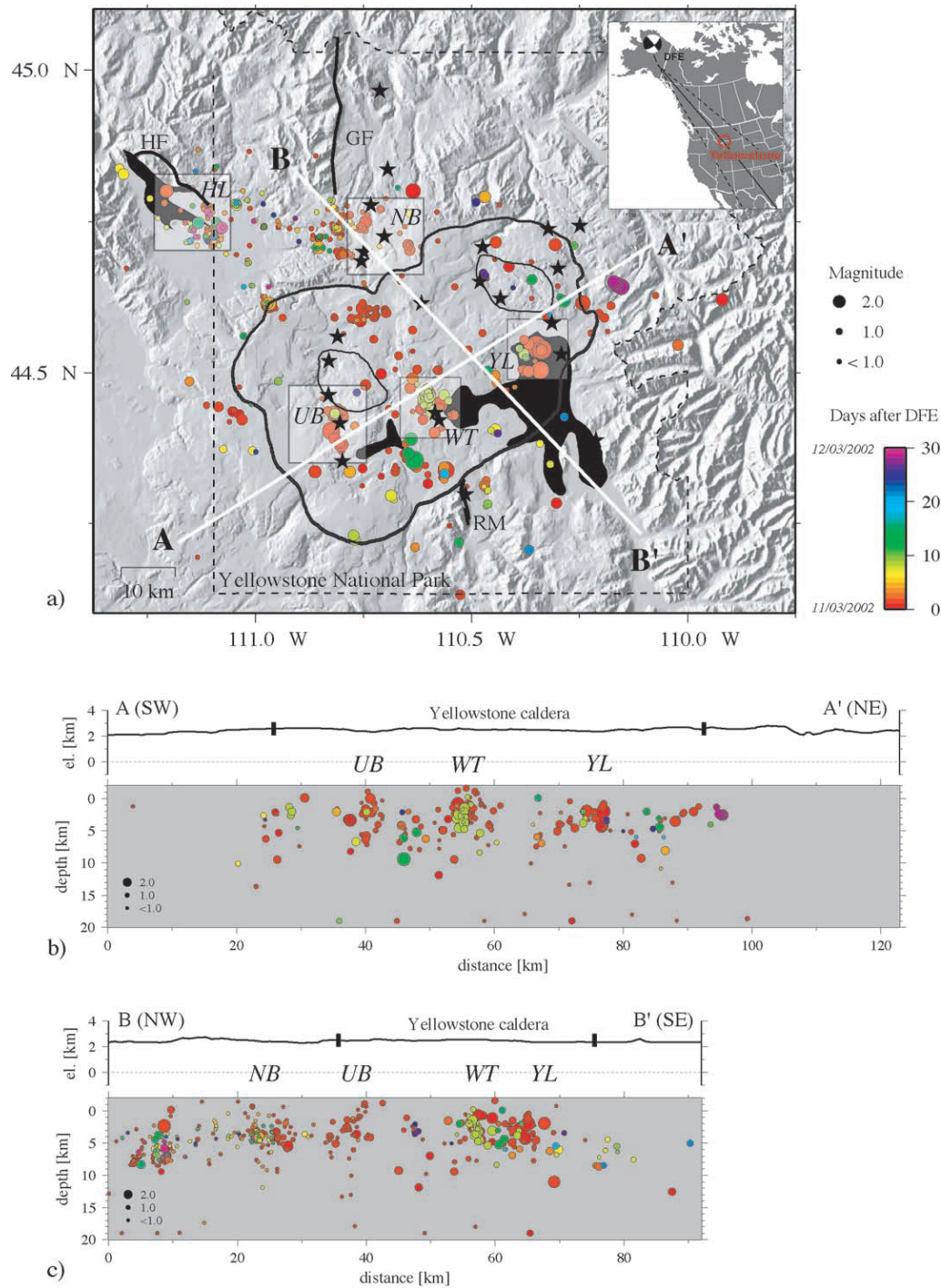


Figure 2. Seismicity within the 1 month after the DFE: a) epicenter locations, b) vertical cross section along profile AA', c) vertical cross section along profile BB'. Hypocenter locations are color coded by time, as indicated, and scaled by coda magnitude,  $M_c$ . Areas that are discussed in the text and shown in Figures 6 and 8 are outlined and labeled: HL, Hebgen Lake area; NB, Norris geyser basin; UB, Upper geyser basin; WT, West Thumb geyser basin; YL, northern end of Yellowstone Lake. Major normal faults are shown by thick black lines: RM, Red Mountain fault zone; GF, Gallatin fault; HF, Hebgen and Red Canyon faults. Inset shows locations of DFE earthquake and Yellowstone in North America. Solid and dashed lines mark the great circle path  $\pm 10^\circ$  along the strike of the Denali fault.

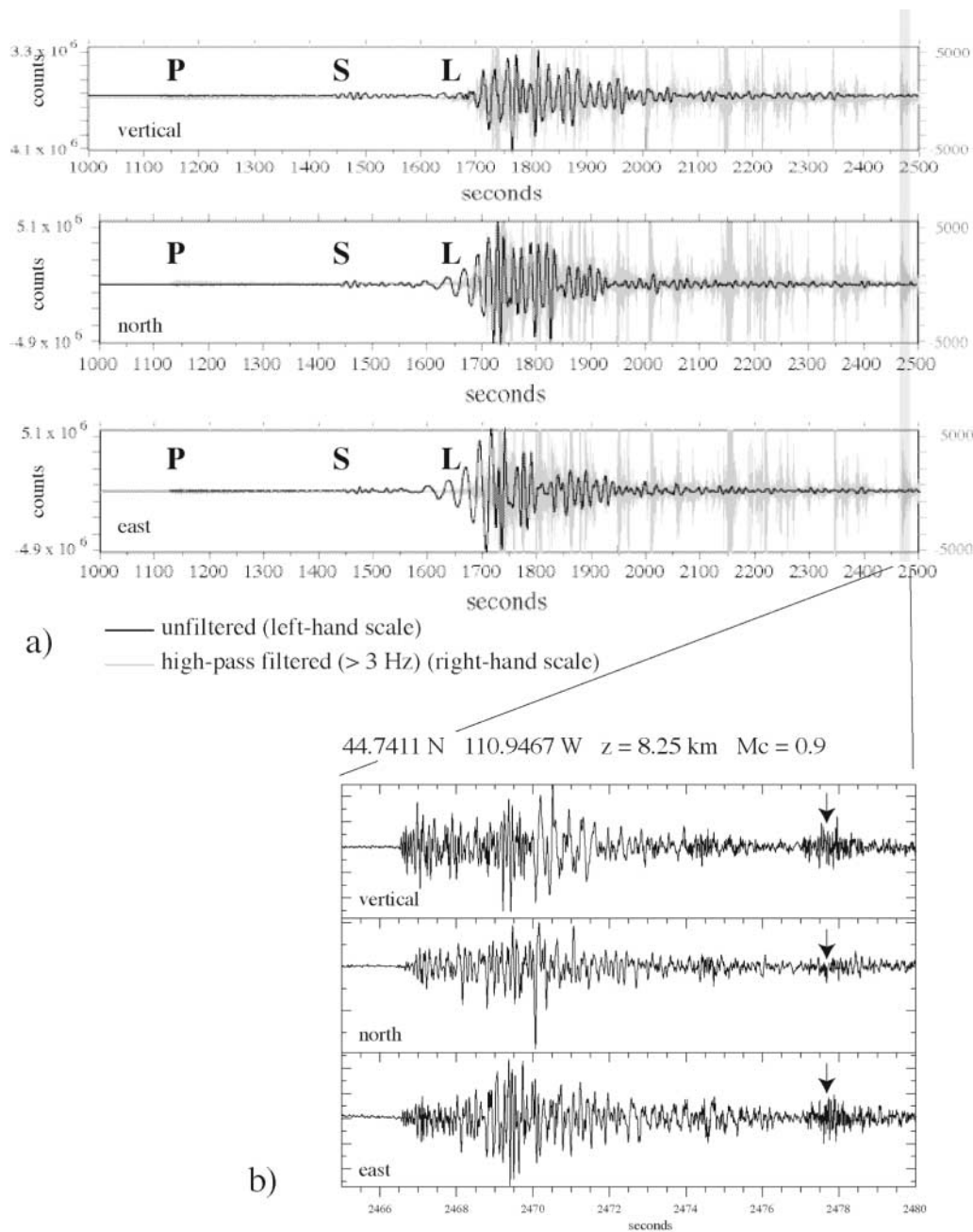


Figure 3. a) Unfiltered (black) and high-pass filtered (gray) seismograms at broadband station YFT (see Fig. 1 for location) of a local earthquake for all three components during the passage of DFE surface waves. Note different scaling for unfiltered and filtered traces as indicated. Major arrivals are labeled: P,  $P$  wave; S,  $S$  wave; L, Love wave. b) High-pass filtered seismogram at broadband station YFT of the local earthquake that could be located as indicated. Arrows mark a second, small, local earthquake in the coda, which could not be located.

quakes) occurred on 11 November 2002, 8 days after the DFE (Fig. 7).

Although considered one of the hottest geyser basins in Yellowstone (White *et al.*, 1988), Norris geyser basin responded differently to the DFE than those geyser basins located inside the Yellowstone caldera. Triggered seismicity

at Norris geyser basin was distributed much more diffusely and was generally deeper (Fig. 8a). In general, the number of larger magnitude earthquakes ( $M > 2$ ) was considerably lower in Norris geyser basin (Fig. 7). The characteristics of triggered seismicity at Norris geyser basin are similar to those in the Hebgen Lake area, which does not show evi-

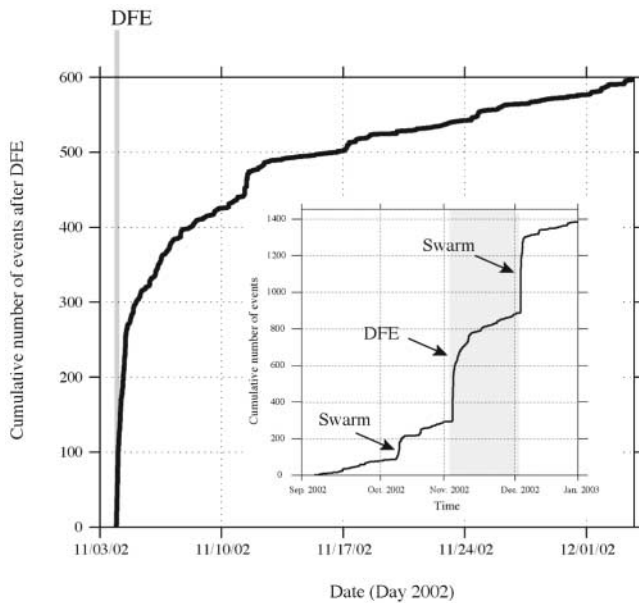


Figure 4. Cumulative number of earthquakes that could be located over a 1-month period following the DFE. Time of DFE is indicated by gray line. Inset graph shows cumulative number of earthquakes 2 months prior to and 2 months after the DFE. Note the occurrence of earthquake swarms prior to and after the DFE. See text on how to distinguish between non-DFE related swarms and seismicity triggered by the 2002 DFE.

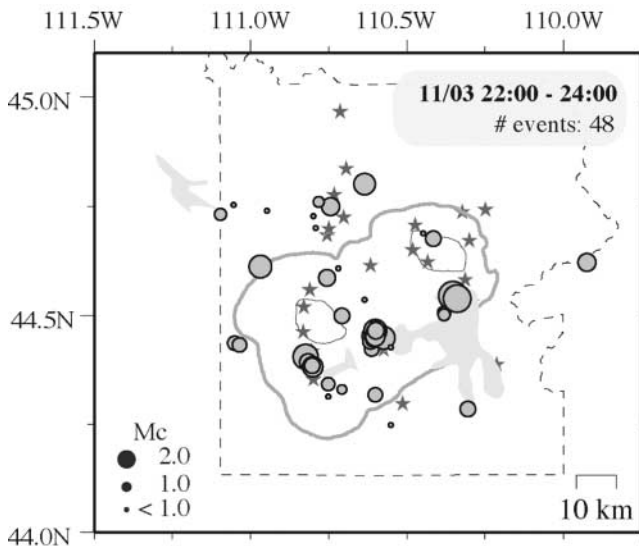


Figure 5. Seismicity triggered during the first 2 hr after the DFE. Epicenter symbols are scaled by magnitude, as indicated. The thick gray line marks the outline of the  $0.64 M_a$  Yellowstone caldera; the thin gray lines mark outlines of resurgent domes. Gray stars mark mapped hydrothermal features. Note the clustering of seismicity close to three major hydrothermal systems within the Yellowstone caldera.

dence for hydrothermal activity. The Hebgen Lake area is dominated by active faulting owing to its proximity to the Hebgen Lake fault, which ruptured in 1959 in a  $M 7.5$  earthquake. Both areas, Hebgen Lake and Norris geyser basin, show a similar diffuse distribution of triggered seismicity (Fig. 8) and a similar magnitude–time distribution, which is remarkably different from that of areas within the Yellowstone caldera (Fig. 7). The differences between earthquake triggering inside and outside the Yellowstone caldera are clearly seen in the cumulative moment release, which is significantly larger for areas inside the Yellowstone caldera (Fig. 9). It is likely that the denser station distribution in the Hebgen Lake area and Norris geyser basin is responsible for the larger number of small earthquakes ( $M < 1.0$ ) in these areas (Fig. 7). However, the difference in seismic moment release is due to a larger number of large-magnitude events ( $M > 2$ ) within the Yellowstone caldera compared with the number outside the Yellowstone caldera (Fig. 7). This suggests that either different trigger mechanisms were acting inside and outside the Yellowstone caldera or that the crust inside and outside the Yellowstone caldera responded differently to the same trigger mechanism.

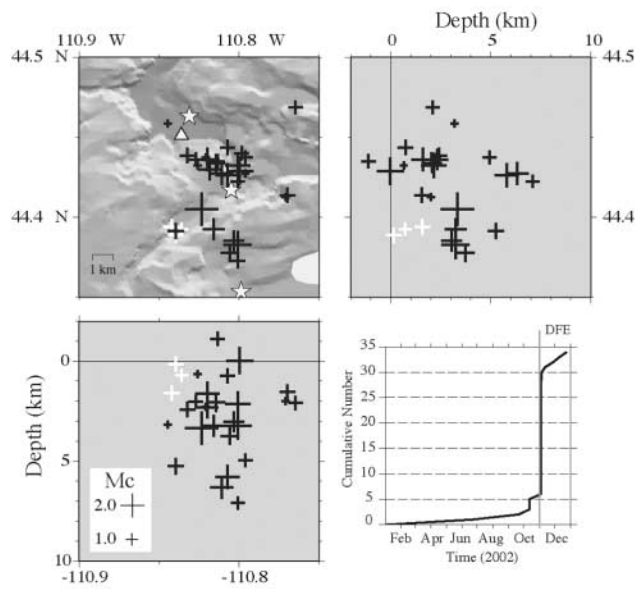
Summarizing the observations on earthquake triggering in Yellowstone following the DFE, we found: (1) The first earthquakes were triggered during the passage of low-frequency, large-amplitude Love waves; (2) earthquake triggering continued well beyond the passage of the DFE surface waves and was widespread in Yellowstone; (3) triggered seismicity decayed gradually over the subsequent weeks except at hydrothermal areas inside the Yellowstone caldera, where triggered seismicity decayed rapidly within 24 hr; (4) early triggered earthquakes ( $< 2$  hr after the DFE) clustered at three major hydrothermal areas inside the Yellowstone caldera; and (5) earthquake triggering showed different characteristics inside and outside the Yellowstone caldera.

### Statistical Analyses of Remotely Triggered Seismicity in Yellowstone

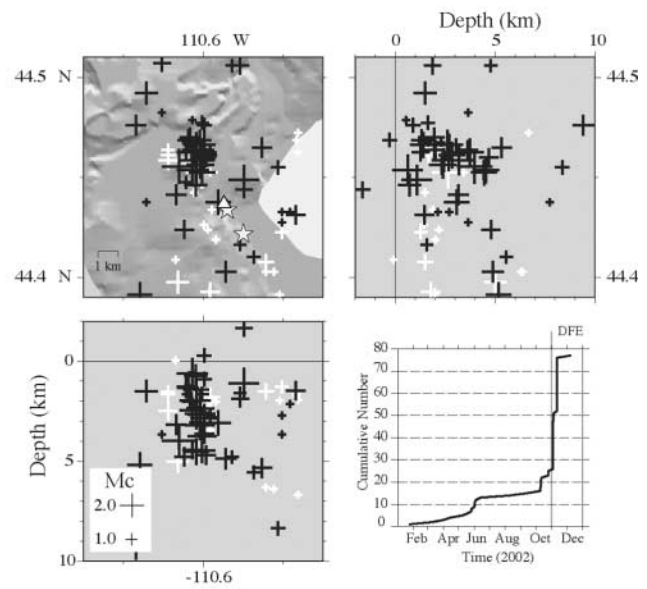
In this section, we analyze the statistical characteristics of the triggered seismicity in detail. We are specifically addressing two questions: (1) How significant and unique is the triggered seismicity? and (2) how long did the triggered seismicity last?

#### Uniqueness and Significance

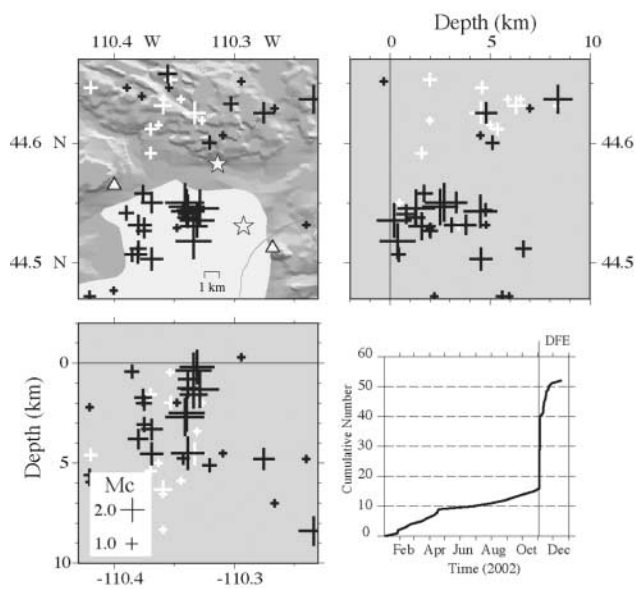
The appearance of local earthquakes immediately following the arrival of the DFE surface waves (Fig. 3) is in itself proof that the triggered seismicity was caused by the DFE. However, we consider it important to establish the statistical significance and uniqueness of the triggering, and to quantitatively compare it with the commonly observed swarm activity in Yellowstone, using the relocated Yellowstone earthquake catalog (Husen and Smith, 2004) from the period January 1994 to June 2003. We limit our analysis to



a) Upper Geyser Basin (UB)



b) West Thumb Geyser Basin (WT)



c) Yellowstone Lake (YL)

Figure 6. Close-up of seismicity triggered close to hydrothermal systems within the Yellowstone caldera: a) Upper geyser basin, b) West Thumb geyser basin, c) northern end of Yellowstone Lake. Hypocenter locations are shown in map view and along two vertical cross sections. Seismicity in 2002 prior to DFE is shown by white crosses; seismicity 1 month after the DFE is shown by black crosses. Gray triangles mark seismic stations of the Yellowstone seismic network; gray stars mark mapped hydrothermal features. Cumulative number of earthquakes in 2002 for each area is shown in the lower right. Time of the DFE is indicated by the gray line.

data collected beginning in 1994; earlier data possess a considerably higher magnitude of completeness, owing to the sparser network prior to 1994. This leaves a total of 16,195 events with magnitudes ranging from  $-1.0$  to  $4.8$ . The data set is not complete for lower magnitudes, but for seismicity rate investigations, homogeneity in reporting, not necessarily completeness, is critical (Habermann, 1987; Zuniga and Wiemer, 1999). Because cutting a catalog at a lower threshold enhances the effect of magnitude shifts on seismicity rates, and also for reasons of simplicity, we begin our investigation using all magnitudes.

When investigating rate changes, earthquake catalogs are commonly declustered to separate clustered seismicity from the assumed independent background seismicity. De-clustering thus reduces the effect of aftershock sequences, foreshock activity, and earthquake swarms. Particularly in volcanic regions such as Yellowstone, earthquake swarms are common and their presence complicates considerably the analysis of seismicity rates. In addition, the declustered catalog is best suited for catalog quality assessment (Zuniga and Wyss, 1995; Zuniga and Wiemer, 1999). The two approaches commonly applied for declustering are Reasenber

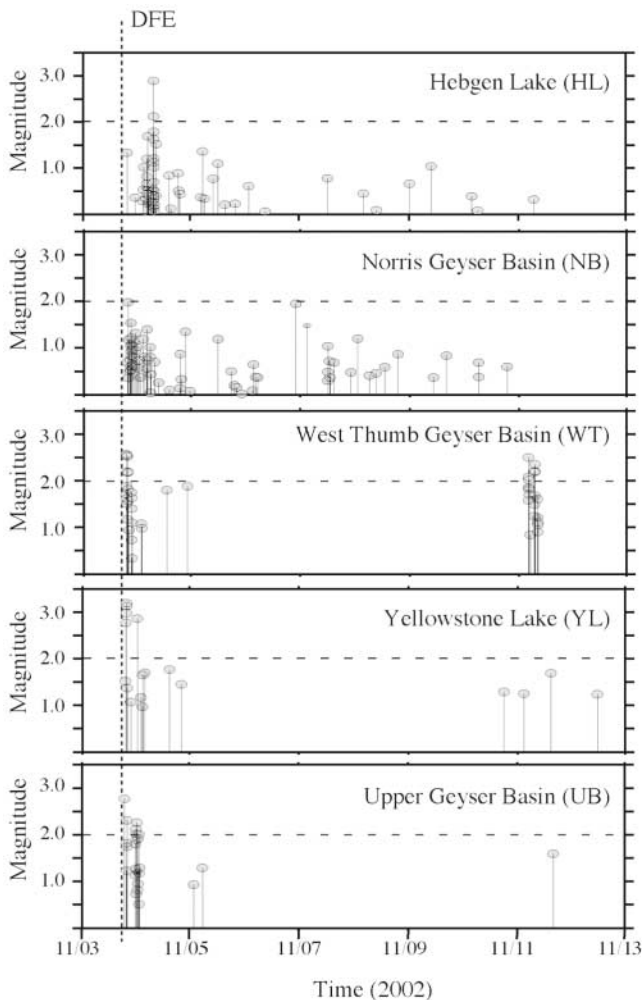


Figure 7. Plot of earthquake magnitude,  $M_c$ , versus time showing the relative rate and size distribution of triggered seismicity for selected areas in Yellowstone. See Figure 2 for the locations of the areas.

declustering (Reasenber, 1985) or a fixed-window approach (Gardner and Knopoff, 1974; Uhrhammer, 1986). Here we apply Reasenber's declustering, because it chooses a more physically based approach to declustering. The algorithm has several free parameters that determine how clusters are linked. We purposely use the original parameters derived for California rather than deriving a region-specific set, because a study of the clustering properties of the Yellowstone seismicity is well beyond the scope of this paper. In addition, by not tuning the declustering process specifically to the DFE triggered events, we achieve a largely unbiased analysis. The declustering algorithm, as implemented in ZMAP (Wiemer, 2001), identifies 1044 clusters, containing 12,434 events. The fact that more than three-fourths of all events are identified as belonging to clusters is not surprising given the frequency of earthquake swarms in the region (Waite and Smith, 2002).

We investigate the homogeneity of reporting of the declustered data set using the GENAS approach outlined by

Habermann (1987) and refined by Zuniga and Wiemer (1999). The GENAS algorithm detects periods of significantly changed reporting in subsamples above and below a prescribed magnitude cutoff. It allows the detection of magnitude shifts, stretches, and rate changes. Applied to Yellowstone, the analysis finds only two periods of significant change, one around mid-1997, and the other related to increase in activity following the DFE. Based on these results, we investigated the annualized rate of events as a function of magnitude bin (Fig. 10) for different periods, using the entire data set (clusters included). If no change in reporting has taken place, these curves should match one other. We compared four periods in Figure 10a. The first period, 1995 to 1997 May, has a somewhat different shape than the subsequent two periods, which could be due to either a small magnitude shift or a change in completeness and simultaneously a change in activity rate. Reporting between the periods May 1997 and the beginning of 2000 and between 2000 and May 2002 remained remarkably constant. The change due to the DFE activity (August 2002–September 2002) can be clearly seen as a strong rate increase of more than a factor of 3, involving all magnitude bands. The peak of the distribution, which is related to the magnitude of completeness, has shifted upward by about 0.5 magnitude unit, suggesting that possibly the completeness deteriorated somewhat during this more active period. However, because regions with  $M_c$  of different completeness (inside and outside the caldera) are combined in this bulk analysis, we prefer an alternative explanation, that the rate change activated the inside and outside differently, as is also indicated by the temporal and spatial evolution of triggered seismicity. Adding more data from a region with poorer completeness will cause an apparent overall deterioration in completeness (Wiemer and Wyss, 2000, 2003).

When separating the seismicity into subsets inside and outside (north) of the caldera, this different degree of activation can be seen very clearly. Inside the caldera (Fig. 10b) the rate increased following the DFE by a factor of about 5; completeness in this area in all periods is estimated to be about 1.5, which was afterward confirmed by an in-depth mapping of  $M_c$  (Wiemer and Wyss, 2000), not shown here for space considerations. Outside, to the north of the caldera, the rate increased by a factor of only 1.7 (Fig. 10c). In this region,  $M_c$  is much lower, at about 0.6. In both regions, however, the post-DFE seismicity follows about the same frequency–magnitude distribution as the pre-DFE seismicity, suggesting that no major change in  $M_c$  has taken place.

To quantify the increase in seismicity following the DFE, we plot seismicity rates both as the cumulative number of earthquakes and as a normalized weekly rate of earthquakes (Fig. 11). This weekly rate is computed as follows:

$$\hat{R}(t_i) = \frac{R(t_i) - \bar{R}}{\sigma}, \quad (1)$$

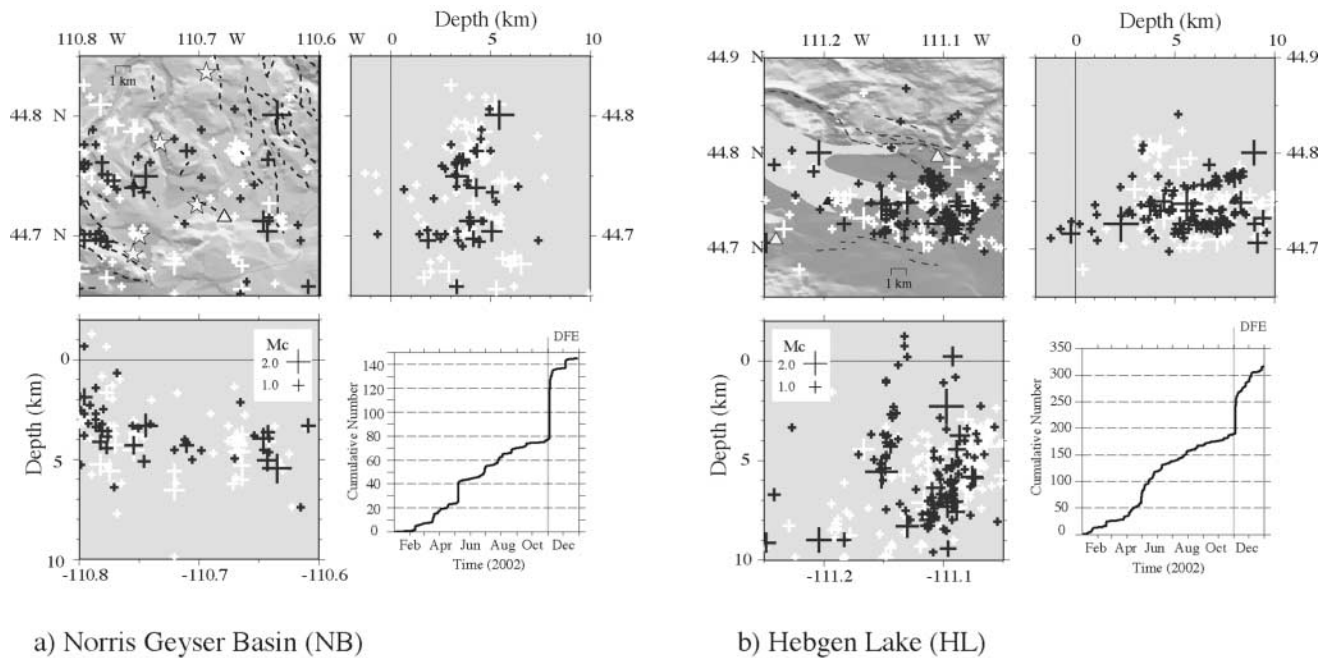


Figure 8. Close-up of seismicity triggered at areas outside the Yellowstone caldera: a) Norris geyser basin, b) Hebgen Lake. See Figure 2 for location of areas. Hypocenter locations are shown in map view and along two vertical cross sections. Seismicity in 2002 prior to DFE is shown by white crosses; seismicity 1 month after the DFE is shown by black crosses. Gray triangles mark seismic stations of the Yellowstone seismic network; gray stars mark mapped hydrothermal features. Dashed lines denote mapped Quaternary faults. Cumulative number of earthquakes for each area is shown in the lower right. Time of the DFE is indicated.

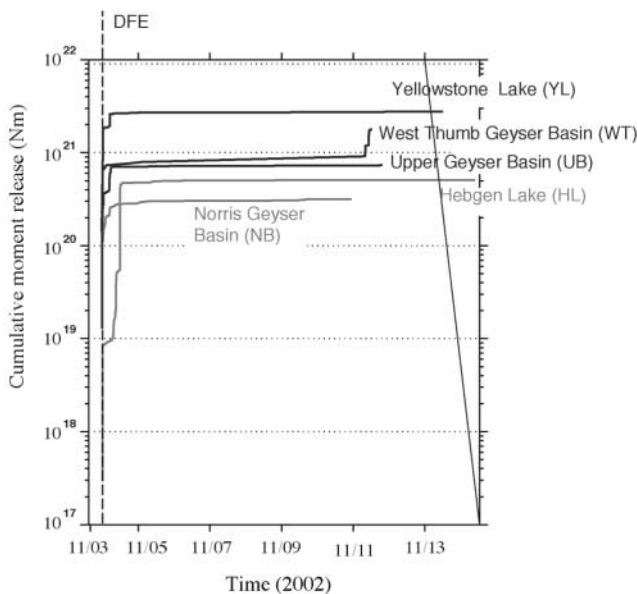


Figure 9. Cumulative moment release at selected areas in Yellowstone. See Figure 2 for the locations of the areas. Cumulative moment release was computed for a 2-week period following the DFE. Time of DFE is indicated by the dashed line. To convert local coda magnitudes  $M_c$  into seismic moment we used a relationship from Puskas (2000).

where  $\bar{R}$  is the mean rate of events per unit time in the time series,  $\sigma$  is one standard deviation, and  $R(Tw, t_i)$  is the rate of events in a window of length  $Tw$  at time  $t_i$ . We compute  $\hat{R}(t_i)$  using a window  $Tw = 7$  days that is moved by one day, resulting in overlapping time windows. A value of three in Figure 11, for example, indicates that a weekly rate change is significantly different from the mean at  $3\sigma$  (0.01 significance) or at the 99.9% confidence level. Our choice of  $Tw = 7$  days is of course somewhat arbitrary; however, we analyzed a wide range of  $Tw$  values and found that the results and interpretation of the significance analysis do not change much. At the time of the DFE, a significant increase ( $\sigma \sim 7$ ) in seismicity was observed (Fig. 11a). However, seven other episodes of significant seismicity rate increases have been observed since 1994.

Plotting the rate of independent (declustered) earthquakes as a function of time reveals (Fig. 11b) that the triggered seismicity following the 2002 DFE now stands out uniquely with a significance of  $30\sigma$ . The declustering smoothed the background seismicity rate such that it can be described well by a stationary Poisson process; the only remaining anomaly is the triggered seismicity following the DFE. In Figure 11c the analysis is repeated for data beginning 1 July 2002. The triggered seismicity appears in the cumulative number plots as a typical decaying sequence, similar to an aftershock sequence. From Figure 11c we es-

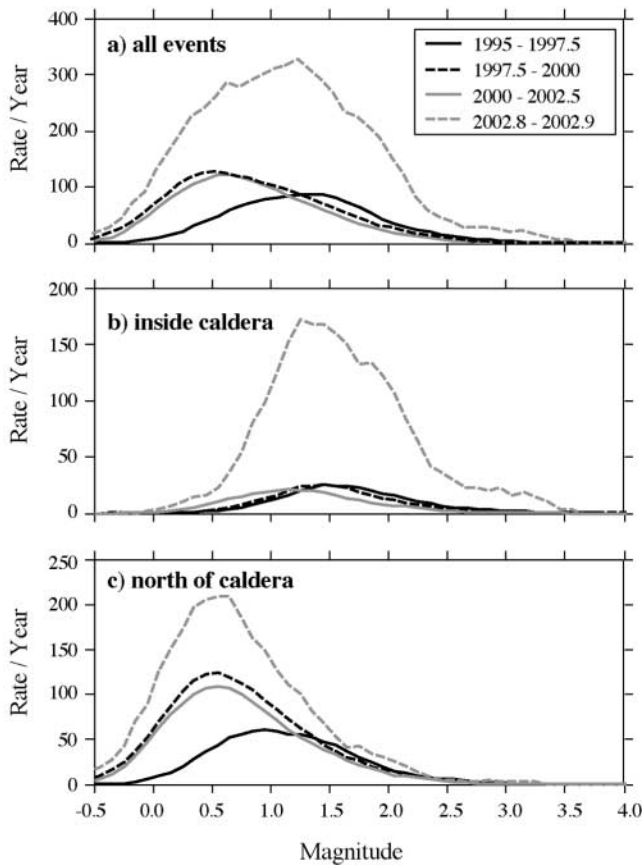


Figure 10. a) Annual rate of earthquakes as a function of magnitude bin. Rates are plotted for four different periods, as indicated in the legend, using all events in the clustered catalog. The rate is normalized to an annual rate by dividing it by the length of the observation period. The gray dashed line corresponds to the post-DFE seismicity; b) same as a), but for events inside the caldera only; c) same as a), but for events outside the caldera.

estimate that in the declustered catalog, about 150 events were triggered in excess of the usual background rate during the first 30 days following the DFE. Therefore, the declustering process removed part of the triggered events, since in the original catalog we found  $>250$  events in the first 24 hr. The fact that the triggered seismicity following the DFE is not removed by the declustering process, as opposed to ordinary earthquake swarms or aftershocks sequences (Fig. 11), offers a criterion by which to distinguish between them.

We also map the spatial distribution of the rate changes, based on the declustered catalog, using the  $\beta$ -function (Matthews and Reasenberg, 1988; Reasenberg and Matthews, 1988), commonly applied to detect and map increases in seismicity rates following large earthquakes (Kilb *et al.*, 2000; Gomberg *et al.*, 2001). We parameterized the volume in overlapping cylinders with a constant radius  $R$  of 10 km, which were spaced 2 km apart in both the  $x$  and  $y$  directions. We computed the  $\beta$ -function comparing the 10-day period following the DFE (11/03/2002 – 11/13/2002) with the back-

ground seismicity prior to the DFE for the period 1 January 1994–2 November 2002. The largest  $\beta$ -values ( $\beta > 14$ ) are found in the southeastern part of the Yellowstone caldera. They decrease gradually to the northwest and are lowest in the northwestern part of Yellowstone. However,  $\beta$ -values are still  $>3$  in most of that region, indicating a statistically significant increase over the background rate. These results are in agreement with the analysis shown in Figure 10: While more events are triggered outside the caldera, the triggering there is less significant when compared to that inside the caldera, because the background rate inside is much lower.

#### Duration of Triggered Seismicity

Establishing the duration of the triggered seismicity is complicated by the fact that it decays into a background of variable seismicity. Because seismicity following the 2002 DFE decayed gradually over time with an appearance of a typical aftershock sequence (Fig. 4), we attempt to fit the decay to a modified Omori law (Utsu, 1961; Ogata, 1983; Utsu *et al.*, 1995; Ogata, 1999):

$$n(t) = k(t + c)^{-p}, \quad (2)$$

where  $n(t)$  is the number of earthquakes occurring at time  $t$ ;  $k$  represents the productivity of the mainshock and depends on the lower magnitude threshold of the given earthquake catalog;  $p$  is a measure of the exponential decrease of the aftershock rate, and  $c$  describes a temporal offset that compensates for incomplete data at the beginning of the aftershock sequence, as well as for a possible physical delaying mechanism. We limited the analysis to magnitudes  $\geq 1.5$ , in order to have a complete data set. A Kolmogorov-Smirnov test is used to evaluate if the fit is acceptable (Woessner *et al.*, 2004).

Using the earthquake catalog over all of Yellowstone, the decay in seismicity could be fitted at a 98% confidence level with the following parameters (Fig. 12):  $p = 1.02 \pm 0.07$ ,  $k = 17.12 \pm 1.96$ , and  $c = 0.0 \pm 0.012$ . When the declustered catalog was used, very similar values were found. These values are well within the observed range for aftershock sequences (Reasenberg and Jones, 1989; Utsu *et al.*, 1995; Wiemer and Katsumata, 1999).

Because the decay in triggered seismicity follows a modified Omori law, we can use the modified Omori law to estimate the duration of remotely triggered seismicity in Yellowstone following the 2002 DFE. By extrapolating the decay (dashed black line in Fig. 12) we find that it intercepts with the constant background rate of 0.7 events per day with  $M \geq 1.5$  (dotted horizontal line in Fig. 12) at about 30 days after the DFE. Thus, remotely triggered seismicity ceased within a month following the 2002 DFE. The same 30-day duration is estimated when using the declustered catalog or when using a higher completeness threshold. The return of the seismicity to the background rate within 30 days suggests

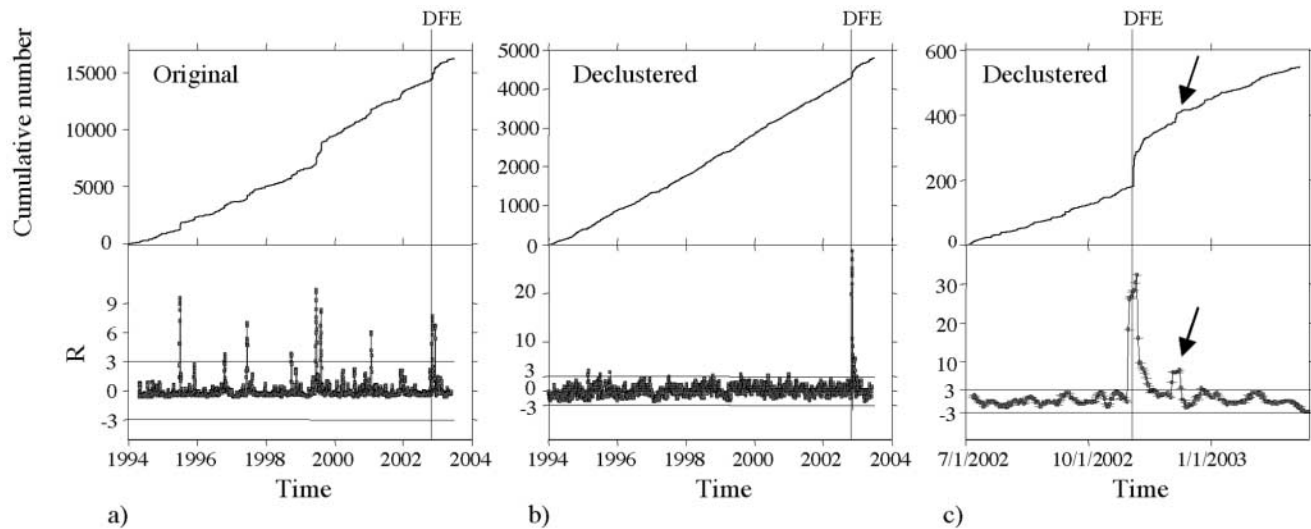


Figure 11. a) Top: Cumulative number of events as a function of time. Data include all events of  $M > 0$  for Yellowstone since 1994. Bottom: Normalized weekly rate of events,  $\hat{R}(t_i)$ , based on the same data. High values indicate significant rate increase in this week as compared to the background rate. Time of DFE is marked by gray line. Seven episodes of significant ( $\hat{R}(t_i) > 3$ ) rate increase are observed in addition to the increase following the DFE. b) Same, but for the declustered data set. c) Same as b, computed for data from 2002 onward only. Arrows mark earthquake swarm on 5 December 2002.

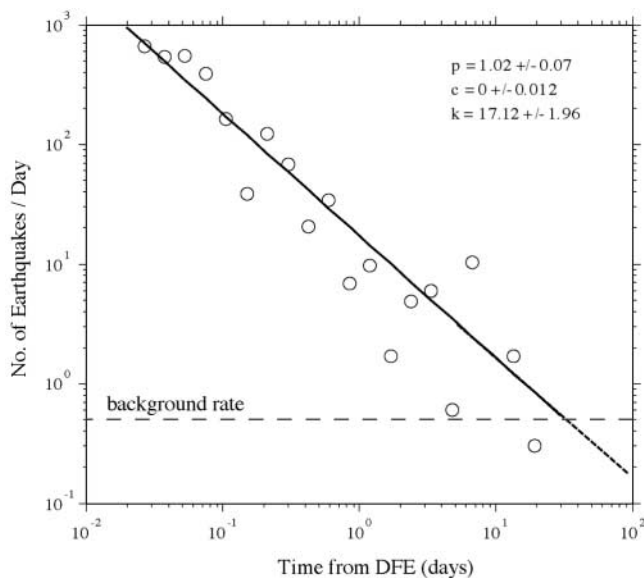


Figure 12. Temporal decay of triggered seismicity following the 2002 DFE for the entire Yellowstone region using the nonclustered earthquake catalog with  $M \geq 1.5$ . Fitting parameters of modified Omori law are indicated. Time from mainshock (horizontal axis) starts at 2 November 2002, 22:26 UTC (arrival of DFE surface waves in Yellowstone). Black dashed line is the extrapolation of the modified Omori law; the dashed horizontal line indicates the average background rate of 0.7 events/day. The intercept of the two lines defines the approximate duration of the triggered seismicity, about 30 days.

that the large earthquake swarm on 5 December 2002 (Fig. 2) was not triggered by the 2002 DFE.

## Discussion

### Comparison with Previous Cases of Earthquake Triggering in Yellowstone and with Other Cases of Earthquake Triggering Following the DFE

The occurrence of the 2002 DFE raises questions as to whether, and how, Yellowstone has responded to previous large earthquakes, such as the 1992 Landers or the 1999 Hector Mine earthquakes. Only a small number (16) of remotely triggered earthquakes were detected following the  $M_w$  7.3 1992 Landers earthquake at a distance of 1250 km (Hill *et al.*, 1993). At that time, however, the Yellowstone seismic network consisted only of one-component, short-period seismometers, and data were transferred to UUSS via analog telemetry lines. During the passage of the Landers surface waves, many of these instruments saturated owing to their low dynamic range. Thus, no local earthquakes could be detected during the passage of the large-amplitude surface waves even using high-pass filtering, which has been proven to be important to detect small earthquakes within the coda of surface waves (Prejean *et al.*, 2004). Furthermore, the Yellowstone seismic network consisted of fewer stations in 1992 than in 2002, and, as a consequence, the magnitude of completeness was considerably higher. Although the Yellowstone seismic network was significantly improved in 1999, we observed no obvious increase in seismicity in Yel-

lowstone following the  $M_w$  7.1 1999 Hector Mine earthquake (Fig. 10). By high-pass filtering the broadband station YMR, located just north of the Yellowstone caldera, we found evidence for five local earthquakes in Yellowstone that may have been triggered during the passage of the surface waves of the Hector Mine earthquake. We were unable to locate these earthquakes since all other stations saturated during the passage of the surface waves. In summary, neither of the two given examples reached a level of earthquake triggering comparable to that observed following the 2002 DFE. Seismicity remotely triggered by the 2002 DFE has been the strongest and best-documented case of remote earthquake triggering in Yellowstone to date.

Varying detection thresholds of the different seismic networks complicates the comparison of triggered seismicity in Yellowstone to that of other areas that experienced seismicity remotely triggered by the 2002 DFE. However, of all the areas that experienced earthquake triggering by the 2002 DFE, only Yellowstone, the Utah region, and the Long Valley caldera, California, exhibited earthquake triggering that continued beyond the passage of the DFE surface waves. At all other areas, triggered seismicity persisted only for a few minutes to hours following the passage of the surface waves, including Mt. Rainier, Washington, the Katmai Volcano Center, Alaska, and the Geysers and Coso geothermal fields, California (Moran *et al.*, 2004; Prejean *et al.*, 2004). At the Long Valley caldera, triggered seismicity occurred mainly as a localized swarm of about 100 earthquakes that started 23.5 hr after the passage of the DFE surface waves and persisted for 17 days. Only Yellowstone and the Utah region exhibited triggering that was persistent over several weeks and distributed over a larger area. Within the first 24 hr after the arrival of the DFE surface waves, 250 earthquakes could be located in Yellowstone compared to 65 earthquakes in the Utah region (Pankow *et al.*, 2004). Over the entire period of elevated seismicity rate (30 days for Yellowstone and 25 days for Utah), 38 earthquakes having  $M > 2.0$  occurred in Yellowstone compared to 24 earthquakes having  $M > 2.0$  in the Utah region. Thus, remotely triggered seismicity in Yellowstone was much more intense despite similar peak dynamic stresses.

The strong directivity of the 2002 DFE can, at least partly, explain the sustained triggering in Yellowstone and in Utah. Peak dynamic stresses measured in Yellowstone (0.2 MPa) and Utah (0.25 MPa) were among the highest observed in the western United States, whereas peak dynamic stresses were considerably lower in California (0.06 MPa) and Alaska (0.1 MPa) (Velasco *et al.*, 2004). Compared to Utah, the higher level and duration of triggered seismicity in Yellowstone suggest that Yellowstone's volcanic nature further amplified remotely triggered seismicity. Volcanic and hydrothermal active areas have been suggested previously to be particularly susceptible to earthquake triggering (Hill *et al.*, 1993; Brodsky *et al.*, 2003). The high sensitivity of hydrothermal systems in Yellowstone to dynamic stress transients is supported by observations of sig-

nificant changes in the eruption behavior of several geysers following the 2002 DFE (Husen, Taylor, *et al.*, 2004).

#### Viable Physical Models Explaining Earthquake Triggering in Yellowstone

Dynamic stress transients associated with low-frequency, large-amplitude surface waves are clearly the dominant triggering mechanism (Hill *et al.*, 1993; Anderson *et al.*, 1994; Gomberg and Bodin, 1994). Static stress changes decay rapidly as a function of distance and fall below tidal stresses at distances of a few fault lengths (Hill *et al.*, 1993). In Yellowstone, static stress changes associated with the 2002 DFE were below 0.0001 MPa (Greg Anderson, personal comm., 2003). At all sites that experienced earthquake triggering following the 2002 DFE, including Yellowstone, the first earthquakes were triggered during the arrival of large-amplitude Love and Rayleigh waves (Fig. 3; see also Pankow *et al.*, 2004; Prejean *et al.*, 2004). Hence, dynamic stress transients seem the most likely causal mechanism. At many sites, however, local seismicity continued well after the passage of the surface waves. Time periods of elevated seismicity ranged from a few minutes at Mt. Rainier (Prejean *et al.*, 2004) to a several weeks in Utah (Pankow *et al.*, 2004) and in Yellowstone (Figs. 4 and 11). Thus, these dynamic stress transients need to be translated into sustained stress changes that are capable of triggering local earthquakes for longer time periods.

Since the 1992 Landers earthquake, several models have been proposed for translating dynamic stress transients into sustained stress changes capable of triggering local earthquakes. They can be grouped into four main classes. The first class changes stresses locally through transient pressurization of crustal magma bodies via advective overpressure of rising bubbles (Linde *et al.*, 1994) or via relaxation of a deep, partially crystallized, magma body (Hill *et al.*, 1995). The second class involves the redistribution of pore pressure due to the rupture of isolated, highly pressurized compartments (Johnston *et al.*, 1995; Brodsky *et al.*, 2003). A third class increases fluid pressure locally through rising gas bubbles (Linde *et al.*, 1994; Hill *et al.*, 2002) or through rectified diffusion (Sturtevant *et al.*, 1996). We note that Ichihara *et al.* (2003) pointed out theoretical problems with rectified diffusion that might reduce the efficiency of earthquake triggering. The fourth class of models changes the mechanical state or properties of existing faults, thus provoking earthquake nucleation (Gomberg *et al.*, 1998; Voisin, 2002). When these models are evaluated with respect to earthquake triggering in Yellowstone, it is important to keep in mind that more than one mechanism might be operating, possibly at different time scales (Prejean *et al.*, 2004).

The 2002 DFE triggered an earthquake series that shows similar characteristics to that triggered in the Long Valley caldera following the 1992 Landers earthquake (Hill *et al.*, 1995). In both cases, triggered seismicity was widespread

over the entire region, persisted for several days, and had a decay that could be fitted with an Omori-type law. Moreover, Long Valley and Yellowstone are both major volcanic calderas in a similar tectonic setting of Basin and Range extension. In Yellowstone, there is also seismological evidence suggesting that a large body of possibly crystallizing magma exists within the middle and lower crust and the upper mantle (Miller and Smith, 1999; Husen, Smith, *et al.*, 2004). Hence, it is plausible to assume similar triggering mechanisms for both systems. One of the preferred models for Long Valley is the relaxation of a deep, partially crystallized magma body at a depth of 50 km (Hill *et al.*, 1995; Johnston *et al.*, 1995). This single mechanism is consistent with triggered seismicity and observed tilt and strain transients within the Long Valley caldera, all with a common temporal evolution. We can neither confirm nor reject a similar model for Yellowstone since data on possible crustal strain and tilt transients are not available. These data have been shown to be essential in locating possible sources of deformation (Hill *et al.*, 1995; Johnston *et al.*, 1995).

Our observation that within the first 2 hr most of the earthquakes were triggered close to major hydrothermal systems inside the Yellowstone caldera suggests that hydrothermal fluids play an important role. This favors models in which pore or fluid pressures are redistributed or locally increased (Johnston *et al.*, 1995; Sturtevant *et al.*, 1996; Hill *et al.*, 2002; Brodsky *et al.*, 2003). These models also have the advantage of explaining the immediate onset and rapid decay of triggered earthquakes. In systems of high permeability such as hydrothermal systems, fluids can be redistributed rapidly, and elevated pore pressure will diffuse relatively quickly. The idea that hydrothermal waters play a critical role for earthquake triggering inside the Yellowstone caldera is further emphasized by the observation that only a few earthquakes were triggered in the northeastern part of the caldera (Fig. 2), where hydrothermal systems are dominated by vapor (Fournier, 1989).

Triggered seismicity outside the Yellowstone caldera exhibited a slower increase and was less intense than that observed inside the caldera (Figs. 7 and 8). Except for in the Norris geyser basin, there is no evidence of hydrothermal activity in the northwestern part of Yellowstone (Fig. 2). Rather, that region is dominated by active Quaternary faulting possibly related to the Hebgen fault and to the Gallatin fault close to Norris geyser basin (Fig. 2) (Smith and Arabasz, 1991; Miller and Smith, 1999). Although we cannot exclude the presence of hydrothermal fluids in that area, it is unlikely that they play a similar role in earthquake triggering to that proposed inside the caldera. This is surprising for the Norris geyser basin, which is one of the hottest geyser basins in Yellowstone and includes one of the largest geysers in the world, Steamboat geyser. One possible explanation is that hydrothermal fluids are restricted to shallow depths and no hydrothermal reservoir exists at intermediate depths beneath the Norris geyser basin. Such hydrothermal reservoirs have been proposed to exist beneath Upper and West Thumb

geyser basins inside the caldera (Fournier, 1989). Clustered hypocenter locations at 3–5 km depth suggests that earthquakes at Upper and West Thumb geyser basins were triggered in the vicinity of such reservoirs (Fig. 6). In contrast, seismicity triggered at Norris geyser basin is more diffuse and slightly deeper (Fig. 8), suggesting that it is related rather to existing faults than to hydrothermal activity. Because seismicity is widespread and faulting is prevalent in the northwestern part of Yellowstone, we propose that the mechanical state or properties of existing faults were altered by the dynamic stress transients of the 2002 DFE, invoking a response governed by the fourth class of models (Gomberg *et al.*, 1998; Voisin, 2002).

From the above discussion we cannot eliminate any of the four models that have been proposed for remote triggering. A viable model must explain the rapid triggering of earthquakes during the arrival of the surface waves, as observed close to hydrothermal systems inside the Yellowstone caldera, as well as sustained earthquake triggering for several days, as observed outside the Yellowstone caldera. Our observations suggest that two or more triggering mechanisms with different timescales are operating simultaneously. This has been proposed for other sites exhibiting triggered seismicity following the 2002 DFE (Prejean *et al.*, 2004). Alternatively, the mechanical state of the crust inside and outside the Yellowstone caldera is likely very different. Temperatures inside the caldera are expected to be much higher, as indicated by a significant shallowing of the background seismicity (Smith and Arabasz, 1991). Thus, it is also feasible that one triggering mechanism is operating with different effects depending on the mechanical state of the medium on which it is acting. With the available data we cannot distinguish between the different scenarios. To do so we need crustal strain measurements, which would place important constraints on how the observed stress transients associated with large-amplitude surface waves translate into strain transients in the seismogenic crust.

## Conclusions

The 2002 DFE triggered a unique and unprecedented seismic sequence in Yellowstone. Although at an epicentral distance of 3100 km from the DFE, it is the best-documented case of remote earthquake triggering in Yellowstone to date. Earthquakes were triggered immediately upon arrival of long-period, large-amplitude surface waves associated with the DFE mainshock. Triggered seismicity continued well beyond the passage of the surface waves, and the seismicity rate was elevated for about 30 days. The temporal and spatial evolution of triggered seismicity in Yellowstone revealed important differences between triggered earthquake sequences inside and outside the Yellowstone caldera. With the available data we cannot distinguish whether different trigger mechanisms operated inside and outside the caldera, or the same trigger mechanism applied to all parts of Yellowstone with different effects depending on the mechanical

state of the crust inside and outside the caldera. However, because triggered seismicity followed the spatial pattern of past seismicity, the observed differences in the characteristics of triggered seismicity might illuminate important characteristics of past seismicity. For example, seismicity triggered close to Norris geyser basin, exhibited characteristics similar to those observed for the Hebgen Lake area, whose seismicity appears to be consistent with active faulting, rather than hydrothermal activity. This suggests that seismicity in Norris geyser basin, in general, is more driven by active faulting than by hydrothermal processes.

Many of the hydrothermal areas inside the Yellowstone caldera experienced strong earthquake triggering. Combined with observed changes of geyser activity following the 2002 DFE (Husen, Taylor, *et al.*, 2004), this indicates that hydrothermal areas in Yellowstone are in a critical state close to failure. Small modifications in the ambient stress can provoke significant changes in seismicity and hydrothermal activity. The near-critical state of Yellowstone is further emphasized by the fact that earthquake triggering was significantly less vigorous throughout nearby Utah, although observed peak dynamic stresses were approximately equal for both regions. Understanding the sensitivity to earthquake-induced stresses of hydrothermal systems such as Yellowstone is important since hydrothermal explosions are considered to be a serious geologic hazard, and more than two million people visit Yellowstone's geyser basins each year.

### Acknowledgments

We are extremely grateful to S. Nava and F. Terra of the University of Utah Seismograph Stations, who picked this difficult data set. We thank Kris Pankow, Stephanie Prejean, Seth Moran, and Emily Brodsky for helpful comments. Reviews by Dave Hill, Charlotte Rowe, and an anonymous referee improved the manuscript significantly. This research was supported by the ETH Zurich, by a cooperative University of Utah–Swiss Science Foundation (Grant 8220-061284) project, the U.S. Geological Survey Volcano Hazard Program, the Yellowstone Volcano Observatory, the NSF Continental Dynamics Program, and the National Park Service, Yellowstone National Park.

### References

- Anderson, J. G., J. N. Brune, J. N. Louie, Y. Zeng, M. Savage, G. Yu, Q. Chen, and D. dePolo (1994). Seismicity in the western Great Basin apparently triggered by the Landers, California, earthquake, 28 June 1992, *Bull. Seism. Soc. Am.* **84**, 844–854.
- Bodin, P., and J. Gomberg (1994). Triggered seismicity and deformation between the Landers, California, and Little Skull Mountain, Nevada, earthquakes, *Bull. Seism. Soc. Am.* **84**, 835–844.
- Brodsky, E. E., V. Karakostas, and H. Kanamori (2000). A new observation of dynamically triggered regional seismicity: earthquakes in Greece following the August, 1999 Izmit, Turkey earthquake, *Geophys. Res. Lett.* **27**, 2741–2744.
- Brodsky, E. E., E. Roeloffs, D. Woodcock, I. Gall, and M. Manga (2003). A mechanism for sustained groundwater pressure changes induced by distant earthquakes, *J. Geophys. Res.* **108**, 2390, doi 10.1029/2002JB002321.
- Christiansen, R. L. (2001). The Quaternary and Pliocene Yellowstone plateau volcanic field of Wyoming, Idaho, and Montana, *U.S. Geol. Surv. Profess. Pap.* 729-G, 145.
- Dzurisin, D., K. M. Yamashita, and J. W. Kleinman (1994). Mechanisms of crustal uplift and subsidence at the Yellowstone caldera, Wyoming, *Bull. Volcanol.* **56**, 261–270.
- Eberhart-Phillips, D., P. J. Haeussler, J. T. Freymueller, A. D. Frankel, C. M. Rubin, P. Craw, N. A. Ratchkovski, G. Anderson, G. A. Carver, A. J. Crone, T. E. Dawson, H. Fletcher, R. Hansen, E. L. Harp, R. A. Harris, D. P. Hill, S. Hreinsdóttir, R. W. Jibson, L. M. Jones, R. Kayen, D. K. Keefer, C. F. Larsen, S. C. Moran, S. F. Personius, G. Plafker, B. Sherrod, K. Sieh, N. Sitar, and W. K. Wallace (2003). The 2002 Denali fault earthquake, Alaska: a large magnitude, slip-partitioned event, *Science* **300**, 1113–1118.
- Fournier, R. O. (1989). Geochemistry and dynamics of the Yellowstone National Park hydrothermal system, *Annu. Rev. Earth Planet. Sci.* **17**, 13–53.
- Gardner, J. K., and L. Knopoff (1974). Is the sequence of earthquakes in Southern California, with aftershocks removed, Poissonian?, *Bull. Seismol. Soc. Am.* **64**, 1363–1367.
- Gomberg, J., and P. Bodin (1994). Triggering of the Little Skull Mountain, Nevada, earthquake with dynamic strains, *Bull. Seism. Soc. Am.* **84**, 844–853.
- Gomberg, J., N. M. Beeler, M. L. Blanpied, and P. Bodin (1998). Earthquake triggering by transient and static deformations, *J. Geophys. Res.* **103**, 24,411–24,426.
- Gomberg, J., P. A. Reasenberg, P. Bodin, and R. A. Harris (2001). Earthquake triggering by seismic waves following the Landers and Hector Mine earthquake, *Nature* **411**, 462–466.
- Habermann, R. E. (1987). Man-made changes of seismicity rates, *Bull. Seism. Soc. Am.* **77**, 141–159.
- Hill, D. P., M. J. S. Johnston, and J. O. Langbein (1995). Response of Long Valley caldera to the  $M_w = 7.3$  Landers, California, earthquake, *J. Geophys. Res.* **100**, 12,985–13,005.
- Hill, D. P., F. Pollitz, and C. Newhall (2002). Earthquake–volcano interactions, *Phys. Today* **55**, 41–47.
- Hill, D. P., P. A. Reasenberg, A. Michael, W. J. Arabaz, G. Beroza, D. Brumbaugh, J. N. Brune, R. Castro, S. Davis, D. dePolo, W. L. Ellsworth, J. Gomberg, S. Harmsen, L. House, S. M. Jackson, M. J. S. Johnston, L. Jones, R. Keller, S. Malone, L. Munguia, S. Nava, J. C. Pechmann, A. Sanford, R. W. Simpson, R. B. Smith, M. Stark, M. Stickney, A. Vidal, S. Walter, V. Wong, and J. Zollweg (1993). Seismicity remotely triggered by the magnitude 7.3 Landers, California, earthquake, *Science* **260**, 1617–1623.
- Husen, S., and R. B. Smith (2004). Probabilistic earthquake location in three-dimensional velocity models for the Yellowstone National Park region, Wyoming, *Bull. Seism. Soc. Am.* **94**, 880–896.
- Husen, S., R. B. Smith, and G. P. Waite (2004). Evidence for gas and magmatic sources beneath the Yellowstone volcanic field from seismic tomographic imaging, *J. Volcanol. Geotherm. Res.* **131**, 397–410.
- Husen, S., R. Taylor, R. B. Smith, and H. Healer (2004). Changes in geyser eruption behavior and remotely triggered seismicity in Yellowstone National Park produced by the 2002  $M$  7.9 Denali fault earthquake, Alaska, *Geology* **32**, 537–540.
- Husker, A., and E. E. Brodsky (2004). Dynamically triggered seismicity in Idaho and western Montana: the necessary geology, *Bull. Seism. Soc. Am.* **94**, no. 6B, S310–S316.
- Ichihara, M., E. E. Brodsky, and H. Kanamori (2003). Reconsideration of the effect of rectified diffusion in volcanic-seismic systems, International Union of Geodesy and Geophysics, General Assembly, Sapporo, Japan Abstract, JSV04/01P/D-001.
- Johnston, M. J. S., D. P. Hill, A. T. Linde, J. O. Langbein, and R. G. Bilham (1995). Transient deformation during triggered seismicity from the 28 June 1992  $M_w = 7.3$  Landers earthquake at Long Valley volcanic caldera, California, *Bull. Seism. Soc. Am.* **85**, 787–795.
- Kilb, D., J. Gomberg, and P. Bodin (2000). Earthquake triggering by dynamic stresses, *Nature* **408**, 570–574.

- Linde, A. T., I. Selwyn Sacks, M. J. S. Johnston, D. P. Hill, and R. G. Bilham (1994). Increased pressure from rising bubbles as a mechanism for remotely triggered seismicity, *Nature* **371**, 408–410.
- Lomax, A., J. Virieux, P. Volant, and C. Thierry-Berge (2000). Probabilistic earthquake location in 3D and layered models, in *Advances in Seismic Event Location*, C. H. Thurber and N. Rabinowitz (Editors), Kluwer Academic Publishers, Dordrecht/Boston/London, 101–134.
- Matthews, M. V., and P. Reasenber (1988). Statistical methods for investigating quiescence and other temporal seismicity patterns, *Pure Appl. Geophys.* **126**, 357–372.
- Miller, D. S., and R. B. Smith (1999).  $P$  and  $S$  velocity structure of the Yellowstone volcanic field from local earthquake and controlled-source tomography, *J. Geophys. Res.* **104**, 15,105–15,121.
- Moran, S. C., J. A. Power, S. D. Stihler, J. J. Sanchez, and J. Caplan-Auerbach (2004). Earthquake triggering at Alaskan volcanoes following the 3 November 2002 Denali fault earthquake, *Bull. Seism. Soc. Am.* **94**, no. 6B, S300–S309.
- Morgan, L. A., W. C. Shanks, III, D. A. Lovalvo, S. Y. Johnson, W. J. Stephenson, K. L. Pierce, S. S. Harlan, C. A. Finn, G. Lee, M. Webring, B. Schulze, J. Duehn, R. Sweeney, and L. Balistreri (2003). Exploration and discovery in Yellowstone Lake: results from high-resolution sonar imaging, seismic reflection profiling, and submersible studies, *J. Volcanol. Geotherm. Res.* **122**, 221–242.
- Nava, S. J., and R. B. Smith (1996). Earthquake catalog for the Yellowstone National Park region, January 1, 1992 to December 31, 1994, with a contribution by R. A. Hutchinson: summary of felt earthquakes in Yellowstone National Park, 1992–1994, *Special Publication*, University of Utah Seismograph Stations, Salt Lake City, Utah, 1–62.
- Ogata, Y. (1983). Estimation of the parameters in the modified Omori formula for aftershock frequencies by the maximum-likelihood procedure, *J. Phys. Earth* **31**, 115–124.
- Ogata, Y. (1999). Seismicity analysis through point-process modeling: a review, *Pure Appl. Geophys.* **155**, 471–507.
- Pankow, K. L., W. J. Arabaz, J. C. Pechmann, and S. J. Nava (2004). Triggered seismicity in Utah from the 3 November 2002 Denali fault earthquake, *Bull. Seism. Soc. Am.* **94**, no. 6B, S332–S347.
- Pechmann, J. C., J. C. Bernier, S. J. Nava, F. M. Terra, and W. J. Arabaz (2001). Correction of systematic time-dependent coda magnitude errors in the Utah and Yellowstone National Park region earthquake catalogs, 1981–2001, *EOS* **82**, F809.
- Pelton, J. R., and R. B. Smith (1979). Recent crustal uplift in the Yellowstone National Park, *Science* **206**, 1179–1182.
- Pitt, A. M. (1987). Catalog of earthquakes in the Yellowstone National Park–Hebgen lake region, Wyoming, Montana, and Idaho, for the years 1973–1981, *U.S. Geol. Surv. Open File Rept. 87-611*, 65.
- Prejean, S. G., D. P. Hill, E. E. Brodsky, S. E. Hough, M. J. S. Johnston, S. D. Malone, D. H. Oppenheimer, A. M. Pitt, and K. B. Richards-Dinger (2004). Remotely triggered seismicity on the United States west coast following the  $M_w$  7.9 Denali fault earthquake, *Bull. Seism. Soc. Am.* **94**, no. 6B, S348–S359.
- Puskas, C. M. (2000). Deformation of the Yellowstone caldera, Hebgen Lake fault zone, and eastern Snake River plain from the global positioning system, seismicity, and moment release, *Master's Thesis*, University of Utah, Salt Lake City, 150 pp.
- Reasenber, P. A. (1985). Second-order moment of central California seismicity, *J. Geophys. Res.* **90**, 5479–5495.
- Reasenber, P. A., and L. M. Jones (1989). Earthquake hazard after a mainshock in California, *Science* **243**, 1173–1176.
- Reasenber, P. A., and M. V. Matthews (1988). Precursory seismic quiescence: a preliminary assessment of the hypothesis, *Pure Appl. Geophys.* **126**, 373–406.
- Smith, R. B., and W. J. Arabasz (1991). Seismicity of the Intermountain Seismic Belt, in *Neotectonics of North America*, D. B. Slemmons, E. R. Engdahl, M. L. Zoback, and D. D. Blackwell (Editors), *Geol. Soc. of Am.*, Boulder, Colorado, 185–228.
- Smith, R. B., and L. Siegel (2000). *Windows into the Earth: The Geology of Yellowstone and Grand Teton Parks*, Oxford University Press, London, 247.
- Stark, M. A., and S. D. Davis (1996). Remotely triggered microearthquakes at the Geysers geothermal field, California, *Geophys. Res. Lett.* **23**, 945–948.
- Sturtevant, B., H. Kanamori, and E. E. Brodsky (1996). Seismic triggering by rectified diffusion in geothermal systems, *J. Geophys. Res.* **101**, 25,269–25,282.
- Uhrhammer, R. (1986). Characteristics of northern and southern California seismicity, *Earthquake Notes* **57**, 21.
- Utsu, T. (1961). A statistical study on the occurrence of aftershocks, *Geophys. Mag.* **30**, 521–605.
- Utsu, T., Y. Ogata, and R. S. Matsu'ura (1995). The centenary of the Omori formula for a decay law of aftershock activity, *J. Phys. Earth* **43**, 1–33.
- Velasco, A., C. Ammon, J. Farrel, and K. L. Pankow (2004). Rupture directivity and its effects of the 3 November 2002 Denali fault earthquake determined from surface waves, *Bull. Seism. Soc. Am.* **94**, no. 6B, S293–S299.
- Voisin, C. (2002). Dynamic triggering of earthquakes: The non-linear slip-dependent friction case, *J. Geophys. Res.* **107**, 2356, doi 10.1029/2001JB001121.
- Waite, G. P., and R. B. Smith (2002). Seismic evidence for fluid migration accompanying subsidence of the Yellowstone caldera, *J. Geophys. Res.* **107**, 2177, doi 10.1029/2001JB000586.
- White, D. E., R. A. Hutchinson, and T. E. C. Keith (1988). The geology and remarkable thermal activity of Norris Geyser Basin, Yellowstone National Park, Wyoming, *U.S. Geol. Surv. Profess. Pap.* **1456**, 84.
- Wicks, J. R., W. Thatcher, and D. Dzurisin (1998). Migration of fluids beneath Yellowstone caldera inferred from satellite radar interferometry, *Science* **282**, 458–462.
- Wiemer, S. (2001). A software package to analyze seismicity: ZMAP, *Seism. Res. Lett.* **72**, 373–382.
- Wiemer, S., and K. Katsumata (1999). Spatial variability of seismicity parameters in aftershock zones, *J. Geophys. Res.* **104**, 13,135–13,151.
- Wiemer, S., and M. Wyss (2000). Minimum magnitude of complete reporting in earthquake catalogs: examples from Alaska, the Western United States, and Japan, *Bull. Seism. Soc. Am.* **90**, 859–869.
- Wiemer, S., and M. Wyss (2003). Reply to “Comment on ‘Minimum magnitude of completeness in earthquake catalogs: examples from Alaska, the western United States, and Japan,’ by Stefan Wiemer and Max Wyss,” by Paul A. Rydelek and I. S. Sacks, *Bull. Seism. Soc. Am.* **93**, 1868–1871.
- Woessner, J., E. Hauksson, S. Wiemer, and S. Neukomm (2004). The 1997 Kagoshima (Japan) Earthquake doublet: quantitative analysis of aftershock rate changes, *Geophys. Res. Lett.* **31**, L03605, doi 10.1029/2003GL018858.
- Zuniga, F. R., and S. Wiemer (1999). Seismicity patterns: Are they always related to natural causes?, *Pure Appl. Geophys.* **155**, 713–726.
- Zuniga, R., and M. Wyss (1995). Inadvertent changes in magnitude reported in earthquake catalogs: influence on  $b$ -value estimates, *Bull. Seism. Soc. Am.* **85**, 1858–1866.

Swiss Seismological Service  
ETH Hoenggerberg  
CH 8093 Zurich, Switzerland  
husen@sed.ethz.ch  
(S.H., S.W.)

Department of Geology and Geophysics  
University of Utah  
Salt Lake City, Utah 84103  
(R.B.S.)